AGU PUBLICATIONS

Geochemistry, Geophysics, Geosystems

RESEARCH ARTICLE
10.1002/2014GC005379

Key Points:
- Low-velocity active landslides are proposed to occur on the seafloor
- Gas hydrates provide a perturbation mechanism for ongoing landslide mobility
- We propose an active, mixed hydrate-sediment seafloor glacier

Correspondence to:
J. J. Mountjoy,
joshu.mountjoy@niwa.co.nz

Citation:
Mountjoy, J. J., I. Pecher, S. Henrys, G. Crutchley, P. M. Barnes, and A. Plaza-Faverola (2014), Shallow methane hydrate system controls ongoing, downslope sediment transport in a low-velocity active submarine landslide complex, Hikurangi Margin, New Zealand, *Geochem. Geophys. Geosyst.*, *15*, 4137–4156, doi:10.1002/2014GC005379.

Received 11 APR 2014
Accepted 7 OCT 2014
Accepted article online 14 OCT 2014
Published online 7 NOV 2014

Shallow methane hydrate system controls ongoing, downslope sediment transport in a low-velocity active submarine landslide complex, Hikurangi Margin, New Zealand

Joshu J. Mountjoy[1], Ingo Pecher[2,3], Stuart Henrys[3], Gareth Crutchley[3], Philip M. Barnes[1], and Andreia Plaza-Faverola[3,4]

[1]National Institute of Water and Atmospheric Research, Wellington, New Zealand, [2]School of Environment, University of Auckland, Auckland, New Zealand, [3]GNS Science, Lower Hutt, New Zealand, [4]Department of Environment and Climate, Centre for Arctic Gas Hydrate, UiT The Arctic University of Norway, Tromsø, Norway

Abstract Morphological and seismic data from a submarine landslide complex east of New Zealand indicate flow-like deformation within gas hydrate-bearing sediment. This "creeping" deformation occurs immediately downslope of where the base of gas hydrate stability reaches the seafloor, suggesting involvement of gas hydrates. We present evidence that, contrary to conventional views, gas hydrates can directly destabilize the seafloor. Three mechanisms could explain how the shallow gas hydrate system could control these landslides. (1) Gas hydrate dissociation could result in excess pore pressure within the upper reaches of the landslide. (2) Overpressure below low-permeability gas hydrate-bearing sediments could cause hydrofracturing in the gas hydrate zone valving excess pore pressure into the landslide body. (3) Gas hydrate-bearing sediment could exhibit time-dependent plastic deformation enabling glacial-style deformation. We favor the final hypothesis that the landslides are actually creeping seafloor glaciers. The viability of rheologically controlled deformation of a hydrate sediment mix is supported by recent laboratory observations of time-dependent deformation behavior of gas hydrate-bearing sands. The controlling hydrate is likely to be strongly dependent on formation controls and intersediment hydrate morphology. Our results constitute a paradigm shift for evaluating the effect of gas hydrates on seafloor strength which, given the widespread occurrence of gas hydrates in the submarine environment, may require a reevaluation of slope stability following future climate-forced variation in bottom-water temperature.

1. Introduction

Active landslides can occur in subaerial environments as low-velocity mass movement complexes that progressively convey sediment downslope by plastic deformation and creep processes [*Hungr et al*., 2001]. Such processes are well documented in weak clay-rich material (often the weathering products of weak rocks) as earthflows/mudflows [*Glastonbury and Fell*, 2008], and in sediment and ice mixtures as rock glaciers [*Haeberli et al*., 2006]. In this context "active" refers to landslide complexes that are continuously or episodically moving residual strength material downslope, as oppose to repeated first time failures (as might occur in a retrogressive landslide). In the submarine environment, low-velocity active landslide processes are little known, with the few published examples including salt-related flow deformation [*Garfunkel et al*., 1979; *Mitchell et al*., 2010], and a submarine landslide complex interpreted as an active earthflow on the Hikurangi Margin, New Zealand [*Mountjoy et al*., 2009]. In the latter example, the authors proposed that stability field perturbations that might enable submarine landslide complexes to maintain activity for prolonged periods include seismic ground-motion, repeated static sediment loading and fluid flow induced pore pressure. Rheological materials that potentially alter sediments to promote viscoplastic, glacier-like creep on submarine slopes include salt, permafrost, and natural gas hydrates.

Gas hydrates are ice-like compounds that occur globally in marine sediments at low temperatures and high pressures [*Kvenvolden*, 1993] in what is known as the gas hydrate stability zone (GHSZ). The base of gas hydrate stability (BGHS) is often visible in seismic data as a bottom simulating reflection (BSR). Gas hydrates have an upslope limit dependent on pressure and temperature conditions where the GHSZ will "pinchout" to the seafloor, and methane hydrate cannot occur in shallower depths than this water depth that we refer

© 2014. American Geophysical Union. All Rights Reserved.

to here as the GHSZ pinchout. Methane in hydrate systems represents a potential energy resource [*Collett*, 2002], and the release of methane to the seafloor may impact global climate [*Kennett et al*., 2003]. Hydrate dissociation is also considered to be a seafloor destabilization mechanism [*Kvenvolden*, 1993; *Lopez et al*., 2010]. The upslope limit of the GHSZ is attracting increased interest in studying the interaction between climatic changes and gas hydrates because gas hydrates in its vicinity are most vulnerable to changes in water temperature [e.g., *Phrampus and Hornbach*, 2012; *Westbrook et al*., 2009] or sea-level [e.g., *Davy et al*., 2010].

The primary mechanism by which gas hydrates have been proposed to influence slope failure is via temperature or pressure-controlled dissociation of hydrate to free gas at the BGHS [e.g., *Kvenvolden*, 1993; *Paull et al*., 1996; *Vogt and Jung*, 2002]. Gas hydrate destabilization is thought to be caused by depressurization with lowered sea level [*Paull et al*., 1991] or by seafloor warming following increases of bottom-water temperatures [*Kennett et al*., 2000; *Phrampus and Hornbach*, 2012]. Hydrate dissociation is widely proposed to result in a significant pore pressure increase in host sediments [*Xu and Germanovich*, 2006] leading to reduced stability of the overlying sedimentary sequence.

Other mechanisms have also been proposed by which the presence of gas hydrates may reduce the static stability of natural slopes. *Sultan et al*. [2004] and *Sultan* [2007] propose that hydrate dissolution at the top of the GHSZ could be an influential factor in marine slope instability. The melting of hydrate, that may itself be increasing shear strength by grain cementation, could lead to localized shear strain due to volume expansion with the creation of shear discontinuities that may act as preferential failure surfaces. Critically overpressured free gas reservoirs may exist at the BGHS in some gas hydrate provinces [*Hornbach et al*., 2004], implying that slopes in these areas might be preconditioned for failure.

Early laboratory results have suggested that gas hydrate is significantly stronger than water ice [*Durham et al*., 2003]. Sediment containing gas hydrate is suggested to be strengthened with respect to adjacent, nonhydrate-bearing sediments [*Winters et al*., 2007], and this cementation effect implies enhanced stability of hydrate-sediment-mix materials. Recent laboratory experiments, however, indicate significant viscoplastic behavior of gas hydrate-bearing sands [*Miyazaki et al*., 2011]. This work shows that incorporating hydrate into a sediment sample may result in significantly enhanced creep behavior, and that hydrate-sediment mixtures may exhibit very high strain-rate dependence. Constitutive modeling based on these recent findings indicates that strain-rate dependence in clay-rich sediments can result in significant strain softening with the implication that the presence of hydrates themselves may reduce the stability of slopes [*Sultan and Garziglia*, 2011].

Gas hydrates thus provide a framework for both generating excess pore pressures within slope sediments and altering the rheology of the seabed. In this study, we analyze newly collected seismic reflection data that show a gas hydrate system intersecting the seafloor within the Tuaheni landslide complex. We elaborate on evidence that this is an active low-velocity landslide complex [*Mountjoy et al*., 2009], and propose three hydrate-related mechanisms for enabling prolonged deformation of the landslide debris.

2. Geological Setting

The study area for this work lies on the upper slope of the northern Hikurangi Margin, off New Zealand's east coast (Figure 1). The region of interest is informally referred to as the *Tuaheni slope*, after Tuaheni Ridge, a structurally controlled seafloor high forming the lower bound to the upper slope basin.

2.1. Tectonic and Stratigraphic Setting

The shelf to continental slope off Gisborne (Figure 1b) is greatly affected by the active tectonic processes of the Hikurangi subduction margin. Oblique convergence between the Pacific and Australian plates at approximately 45 mm/yr is partitioned into lateral motion in the onshore axial ranges and orthogonal convergence across the offshore subduction system [*Wallace et al*., 2004]. Offshore active faults occur as pure dip-slip thrust faults striking parallel to the margin in two primary zones, from the deformation front to the midslope, and from the outer continental shelf to the coast [*Mountjoy and Barnes*, 2011]. From the midupper slope, there is a gap in active structures, along at least 100 km strike-length of the margin. The activity of faults underlying the continental shelf is well documented, with vertical rates of 3–5 mm/yr [*Mountjoy and Barnes*, 2011]. Although the specific activity of upper-plate faults underlying the midlower slope are not well known, in terms of ground shaking potential, all upper plate faults and the Hikurangi subduction thrust

© 2014. American Geophysical Union. All Rights Reserved.

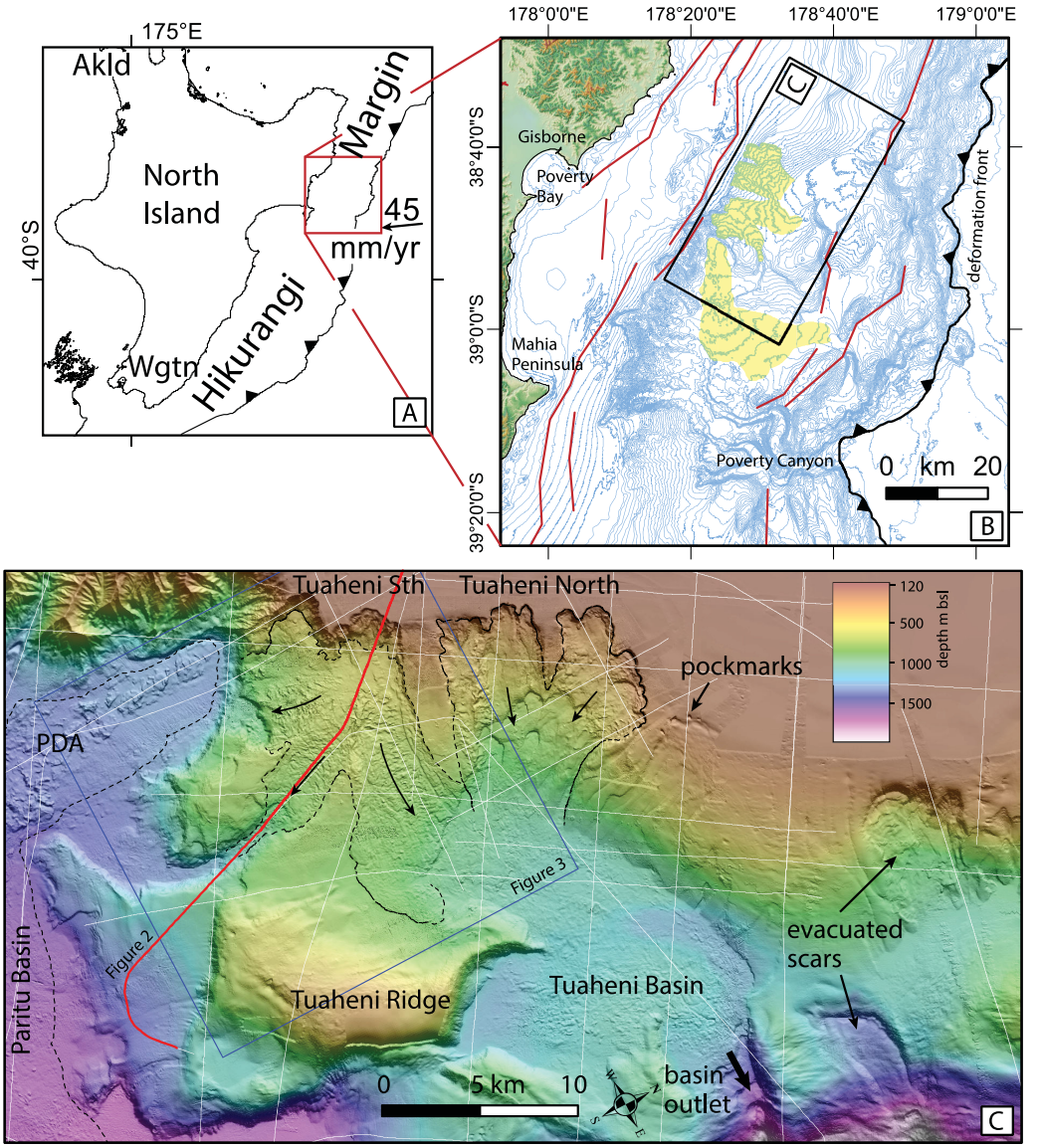

Figure 1. Study area location, main tectonic features, and slope geomorphology. (a) Location of study area on the Hikurangi Margin. Plate motion vector from *Beavan et al.* [2002]. (b) Forearc geomorphology and principal tectonic features, showing the deformation front, active (upper plate) earthquake sources (red) after *Stirling et al.* [2012], and distribution of major mass transport deposits exposed on the seafloor (yellow) after *Mountjoy et al.* [2009] and *Mountjoy and Micallef* [2012]. (c) Local geomorphology, physiographic features, and geophysical data available in the study region. Underlying multibeam bathymetry is a compilation of Kongsberg EM300 and EM302 data sets. White lines show available seismic reflection profiles. Red line indicates the location of composite seismic reflection profile in Figure 2. Blue outline indicates the extent of Figure 3. Black arrows indicate the direction of movement within the slides. PDA refers to the Paritu Debris Avalanche [*Mountjoy and Micallef*, 2012].

are accounted for in the National Seismic Hazard Model (NSHM) [*Stirling et al.*, 2012]. Earthquake sources in the study area are indicated in Figure 1b as red lines, and the NSHM indicates the peak ground acceleration (PGA) of 0.4–0.5 g at a 250 year return period across the upper slope.

The Tuaheni slope is underlain by Quaternary shelf-edge clinoform sequences that extend from the outer shelf onto the upper slope [*Pedley et al.*, 2010]. The clinoforms are characterized by wedge-shaped, gently dipping, parallel bedded sedimentary packages and are characteristic of sea-level-cycle controlled progadational deposits, i.e., the lowstand systems tract [e.g., *Posamentier and Vail*, 1988; *Van Wagoner et al.*, 1988]. The clinoform sequences are fine grained at the surface [*Alexander et al.*, 2010], reflecting Holocene sedimentation, but likely contain a significant sand fraction at depth as documented for equivalent clinoform sequences near-by [*Barnes et al.*, 1991]. The Quaternary sequences are underlain by Miocene and older

© 2014. American Geophysical Union. All Rights Reserved.

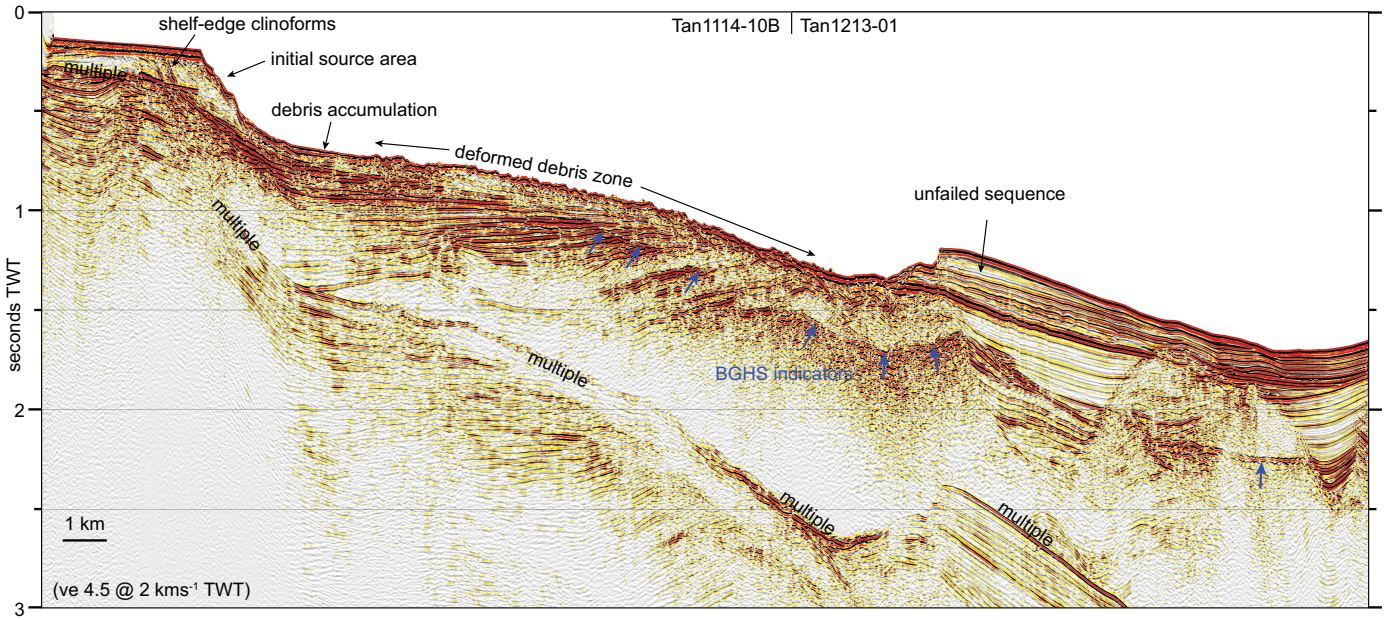

Figure 2. Regional seismic line illustrating the shelf break to upper slope sedimentary setting, the contrast between failed seabed (deformed debris zone) and intact slope stratigraphy (unfailed sequence). Bottom simulating reflections (BSRs) represent the base of gas hydrate stability (BGHS)—blue arrows. The line is located in Figure 1c.

rocks that are variably exposed by erosion and tectonic uplift [*Barnes et al*., 2002; *Field et al*., 1997; *Mountjoy and Barnes*, 2011].

2.2. Previous Work on Gas Hydrates

The Hikurangi Margin east of the North Island of New Zealand is likely to hold significant accumulations of hydrates [*Navalpakam et al*., 2012; *Pecher and Henrys*, 2003]. A possible link between gas hydrates close to the upper limit of the GHSZ and seafloor erosion has been proposed for a location known as Rock Garden, south of the study area [*Crutchley et al*., 2010; *Ellis et al*., 2010; *Pecher et al*., 2005]. Rock Garden is a subseafloor ridge with a plateau-like top that is flanked by BGHS pinchouts. Two mechanisms have been proposed to link gas hydrates and seafloor erosion to explain its flattened ridge top. (1) Repeated formation and dissociation of gas hydrates ("freeze-thaw" cycles) due to water-temperature fluctuations may lead to repeated expansion and contraction of pore volumes, thereby fracturing the seafloor. (2) Overpressure from fluid migration beneath a very shallow, low-permeability gas hydrate zone may lead to hydrofracturing in the shallow subseafloor. Results from modeling favor the second concept [*Crutchley et al*., 2010; *Ellis et al*., 2010]. In both models, fracturing would weaken the seafloor. Weakened material could then be transported away by currents.

2.3. Tuaheni Slope Instability

Submarine slope instability is widely recognized along the length of the Hikurangi Margin [*Barnes et al*., 2010; *Collot et al*., 2001; *Faure et al*., 2006; *Kukowski et al*., 2010; *Micallef et al*., 2012; *Mountjoy et al*., 2009; *Mountjoy and Micallef*, 2012; *Pedley et al*., 2010]. The continental slope off the coast of Gisborne is subject to widespread mass failure, including some of the largest and best preserved landslide complexes on the margin. The Tuaheni landslide complex occurs within the outer-shelf to upper-slope clinoform sediments on the Tuaheni slope (Figures 1c and 2). The surface morphology of the ~145 km^2 landslide complex is described in detail by *Mountjoy et al*. [2009]. First-order landslide morphological features are clearly delineated, including headscarps (source areas) and landslide deposits. The base of the Tuaheni landslide is stratigraphically controlled, with a planar basal failure surface which steps down to deeper horizons down the landslide length (Figure 2). Debris above the basal failure surface exhibits tectonic-style deformation, transitioning from contraction in the upper slide debris to extension in the lower slide debris region. These morphologic features, together with nested lateral shear zones and significant deflation in the main

© 2014. American Geophysical Union. All Rights Reserved.

landslide track, closely resemble creep deformation features observed in terrestrial earthflows [*Mackey et al*., 2009].

The landslide comprises two distinct components (north and south) which primarily contribute failed material to the debris-filled Tuaheni basin, with a component feeding into the Paritu basin (Figure 1c). *Mountjoy et al*. [2009] recognized that the landslide complex is dominated by stratigraphically controlled failures and recognized some key differences between the north and south domains. Tuaheni North is dominated by multiple, overprinted landslide scars between 700 and 1800 m across. Scarp heights are predominantly around 100 m, sloping at approximately 8–20°, and occur from 150 to 850 m water depth. The evacuated scars in Tuaheni North contain minimal landslide debris suggesting that, following failure, debris was mostly conveyed to the Tuaheni basin, the floor of which is at water depths between 900 and 1000 m. In contrast, source area scars in Tuaheni South occur near the shelf break, in water depths of 150–550 m. These scars are >2500 m wide, with 300–350 m high scarps sloping at 8–20°. Downslope of the Tuaheni South source-area-scars, an 80 km^2 field of irregular, rough landslide debris is observed at depths between 550 and 850 m, sloping at 1.5–4°. An arcuate apron of debris containing transverse contractional folds is interpreted as a remnant of the parent landslide proposed to from an initial, relatively rapid slope failure. The lower boundary (toe) of the debris field is predominantly unconfined. Kinematic indicators from surface morphology show three directions of movement, partitioning the slide into three separate components (Figure 1c).

Based on morphometric analysis of the surface roughness of the Tuaheni South landslide debris, combined with interpretation of subsurface features in multichannel seismic data, *Mountjoy et al*. [2009] identified multiple features that indicate compression, extension and lateral-shear deformation. Considering (1) the distribution of contractional versus extensional deformation (extension occurs in the distal slide region as oppose to the upper region of the slide as is most common for single event or stacked failures on land and on the seafloor), (2) the very well formed lateral shear zones, (3) the lack of vertical partitioning of the slide debris, and (4) the similarity of the surface morphology with other creep-dominated slope deformation processes on-land, the authors propose that this landslide complex is a submarine earthflow subject to perturbations inducing ongoing mobility. Earthflows are landslide complexes in areas of weak, clay-bearing rock that behave as slow, glacier-like debris streams that repeatedly remobilize the same material [*Baum et al*., 2003; *Hungr et al*., 2001]. While the mobility of terrestrial earthflows is principally controlled by precipitation-controlled elevations in pore pressure, this clearly does not influence submarine slopes. *Mountjoy et al*. [2009] proposed that the ongoing mobility, either episodic—stick-slip—or continuous creeping motion could be controlled by earthquakes, gas expulsion, or rapid sediment loading, all of which might plausibly occur at this site. Gas hydrate indicators in the vicinity of the landslides were not, however, identified in this previous study.

A newly available grid of high resolution multichannel seismic reflection data now provide significant further insight into these landslides. The new data confirm and further constrain the nature and extent of creeping and show shallow gas hydrate indicators below the landslides (Figure 2), as identified by *Navalpakam et al*. [2012] on the adjacent slope. Based on interpretation of the new seismic reflection data, we propose a mechanism for the long-term deformation behavior of actively mobile submarine landslide complexes in gas hydrate provinces.

3. Data

3.1. Multibeam Bathymetry

The Tuaheni slope is extensively mapped with Kongsberg Simrad EM300 and EM302 30 kHz multibeam bathymetric data (Figure 1c). Simrad EM300 data were collected with the hull-mounted instrument on *RV Tangaroa* in 2006 and 2008. The system operates 135 1 × 2° beams at 30 kHz. Shipboard navigation comprises a POS/MV system with differential GPS. A grid size of 25 m is chosen to honor beam insonification and sounding density across the water depths of interest. EM300 data were processed to this resolution in Hydromap. Kongsberg EM302 data were collected in 2011 with the upgraded hull-mounted instrument on *RV Tangaroa*. The EM302 system operates 288 1 × 2° beams at 30 kHz, and employs the same navigation system as previously. Data were processed on board using CARIS HIPS & SIPS and QPS Fledermaus, and gridded at 25 m.

© 2014. American Geophysical Union. All Rights Reserved.

3.2. Seismic Reflection

A significant amount of seismic reflection data is available in the study area (Figure 1c). This includes unpublished multichannel seismic reflection data (MCS) collected in 2011 [*Barnes et al*., 2011] and 2012 [*Wysoczanski et al*., 2012]. For both surveys, data were collected with the same system aboard *RV Tangaroa*. The seismic system has a 600 m streamer with 48 channels and a group interval of 12.5 m. Depth is controlled by a CSMX system with compass birds providing streamer feather angle information. Navigation is via Hydropro navigation software from Trimble to merge depth, DGPS position (POSMV antenna accurate to $\pm$0.4 m). The seismic source is a dual GI gun (2 $\times$ 45/105 cubic in.).

In addition, archived MCS data are available, including GeodyNZ 6-channel seismic reflection data collected in 1993 [*Collot et al*., 1996], TAN0106 24-channel NIWA survey data collected in 2001 [*Mountjoy et al*., 2009; *Pedley et al*., 2010], and 05CM New Zealand Government-funded deep-penetration petroleum industry survey data collected in 2005 [*Multiwave*, 2005; *Navalpakam et al*., 2012].

3.3. Oceanographic

The study area is broadly located in a zone of mixing between the cooler Wairarapa Current that travels northward along the North Island's east coast and the warmer East Cape Current approaching the North Island from the north. This mixing is thought to lead to the Wairarapa Eddy causing mesoscale (100–200 days) temperature fluctuations [e.g., *Chiswell*, 2005]. Historic CTD data within $\sim$100 km of Rock Garden, approximately 140 km south of the Tuaheni area [*Pecher et al*., 2005], as well as a $>$450 day mooring deployment close to Rock Garden suggest bottom-water fluctuations of almost $\pm$1°C. [*Pecher et al*., 2008]. Historic CTD measurements within $\sim$100 km of the Tuaheni area display similarly large fluctuations with average temperatures that are only $\sim$0.1°C lower than those on Rock Garden.

3.4. Surface and Subsurface Landslide Morphology

Key elements of the landslide, including the depth of failure plane, slope gradient, and the affected area and volume were all described by *Mountjoy et al*. [2009]. While full coverage multibeam bathymetry data were available to these authors, new Kongsberg-Simrad EM302 data are less noisy and, with the higher sounding density of this instrument, provide significantly improved resolution imaging of landslide surface morphology (Figure 3). The same features identified as diagnostic of creeping deformation are observed more clearly in the new multibeam data. The uninterpreted multibeam bathymetry insets in Figure 3 illustrate the complex surface morphology of the landslides, including crescent-shaped concave downslope fracture/scarp features and linear lateral scarps indicating faulting and folding of the landslide debris.

New seismic reflection data provide significant insight into the internal structure of the landslides. The geometry of seismic reflections can indicate sediment deformation style in terms of contractional and extensional deformation, the character of which is exemplified by the internal deformation of large-scale gravity instability systems [e.g., *de Vera et al*., 2010; *Maloney et al*., 2012]. The Tuaheni slides exhibit the characteristic rollover and stacking geometries related to thrust fault development and contractional folding, and down-dropping resulting from extensional faulting (Figures 4 and 5). Deformation structures indicate contractional deformation in the upper regions of the slides and extensional deformation in the distal (downslope) parts. The boundary between contractional and extensional areas is in agreement across the different slide components (Figure 3). Quantifying the dip angle of the faults shown in Figures 4 and 5 demonstrates that contractional faults have an average dip of 29° while extensional faults have an average dip of 63°. The clear distinction of the dip populations between reverse and normal faults is indicated in Figure 6. The measured dip values for both fault populations are characteristic of low angle thrust (contraction) and dip slip (extension) [*Scholz*, 2002], supporting the downslope distinction between deformation domains as shown in Figures 3–5.

Deformation features within the debris sole to a basal surface defined by relatively coherent underlying reflectivity, and higher amplitude reflections. Material directly beneath the deforming debris contains features that indicate it is also landslide material. It onlaps or is discontinuous with upslope material, and contains contractional deformation structures (Figures 4 and 5). We thus recognize two stratigraphic units within the Tuaheni landslides, (1) a lower unit of semi-coherent higher amplitude reflectivity forming a wedge that completely tapers out downslope and (2) an overlying highly disrupted, low amplitude surface unit that retains a relatively constant thickness downslope but which varies locally from 60 to 130 m.

© 2014. American Geophysical Union. All Rights Reserved.

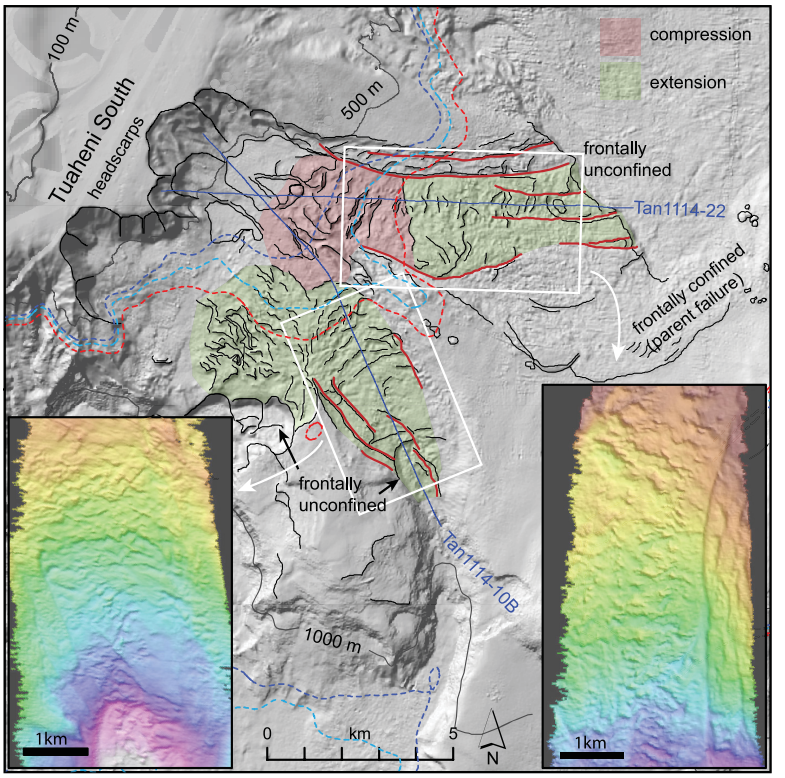

Figure 3. Geomorphology of the Tuaheni landslides. Black linework indicates a deformation-related contractional and extensional features within debris bodies after *Mountjoy et al*. [2009]. Red lines are lateral shear faults. Red transparency indicates a contractional region in the debris field, and green transparency indicates an extensional region. Colored insets show an uninterpreted single-swath multibeam data across the lower extensional zones of the two main components of the landslide. The location of seismic reflection profiles presented in Figures 4 and 5 is indicated. Dashed contour lines show the highest probability seafloor intersect of the BGHS (605 m, light blue), and the minimum (585 m, dark blue) and maximum (640 m, red) depth. Colors are as per Figures 8 and 9 and are discussed in the text in section 5.4.

Underlying these units, a >300 m thick sequence of coherent, horizontal to gently landward-dipping stratigraphy represents the intact sequence of the clinoform sediments deposited in the upper slope.

3.5. Gas Hydrate System Geometry and Dynamics

The main seismic indicator of the gas hydrate system is exemplified by a BSR crossing landward dipping reflections (Figure 2). Dipping, high-amplitude reflections beneath the GHSZ that terminate at the BSR are classical indicators of gas charged sediments [*Berndt et al*., 2004]. To gain a more regional understanding of gas hydrate stability, we analyzed all available multichannel seismic data sets in the areas surrounding the Tuaheni landslide and picked BGHS indicators where they are easily identifiable. The depth of BGHS seismic indicators below the seafloor with respect to modeled curves indicate upper and lower geothermal gradients for hydrate stability of 20 and 65°C km^{-1} (Figure 7). The average value of 30°/km is in good agreement with the local model-fit value for the BGHS beneath the Tuaheni Landslides of 27°C km^{-1}.

We do not observe any clear evidence for BGHS pinchouts with the seafloor in seismic reflection data within the Tuaheni slide area. However, we identified two possible reflections that may mark the BGHS pinchout: a weak reflection that appears to be cutting through stratigraphic layers and may pinch out at the seafloor at ~560 m depth (Figure 4) and a reflection that appears to cut through stratigraphy pinching out at 645 m (Figure 5). Both reflections are unusually weak for gas-related BSRs and we were not able to unambiguously establish their polarities. We therefore do not consider these events as reliable indicators for BGHS pinchouts, and predict seafloor positions of the BHGS (green line in Figures 4 and 5) based on BSR depth beneath the seafloor as a function of water depth further downslope. This water depth position is in agreement with the numerous BGHS pinchouts on the flanks of Rock Garden at 630–645 m water depth [*Crutchley et al*., 2010; *Pecher et al*., 2005].

© 2014. American Geophysical Union. All Rights Reserved.

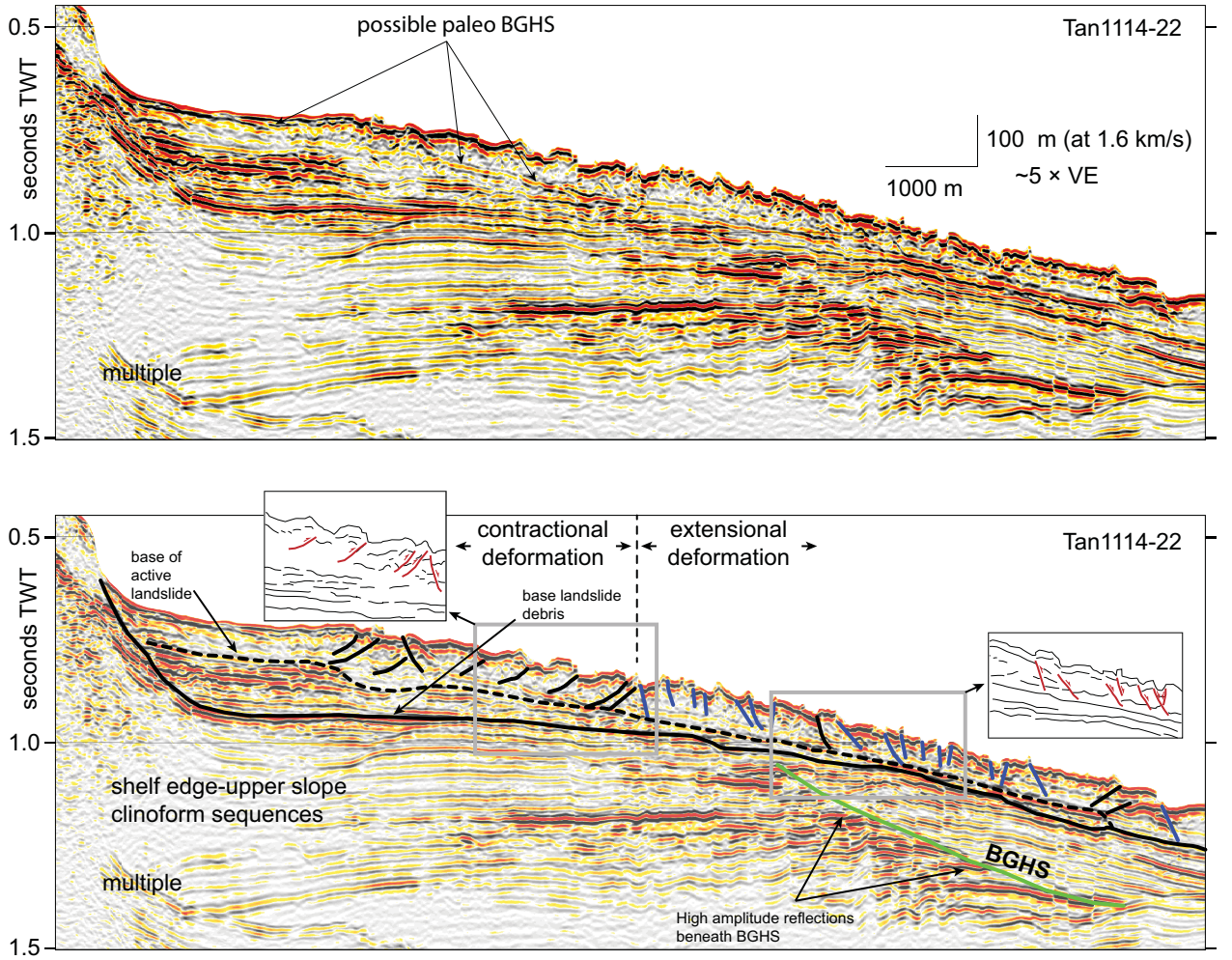

Figure 4. Uninterpreted and interpreted versions of true-amplitude multichannel seismic profile Tan1114-22 down the length of the Tuaheni landslide. Features mapped include the base of landslide debris (solid black line), the interpreted base of active deformation (dashed black line), and the base of gas hydrate stability (BSR, green), internal landslide deformation features (black). Linework interpretations show an internal reflectivity indicative of faulting style.

To model the stability and subsurface location of the gas hydrate phase boundary, we assumed a system without any recent sediment removal or deposition and with constant water temperatures as a function of time. Water temperature was assumed to decrease with depth following the average temperature profile observed in CTDs (Figure 8). For our initial estimate of the depth of the BGHS as a function of water depth, including depth at the seafloor, we assumed a thermal gradient of 0.025°C m^{-1} based on observations elsewhere along this margin [*Pecher et al.*, 2010] and used physical and chemical properties as listed in Table 1 [after *Pecher et al.*, 2005]. We then tried to match observed and predicted depth of the BGHS by varying the thermal gradient and adding constant values to water temperatures. The latter accounts for both unknown precise water temperatures as well as changes in the composition of gas and pore water, which lead to near-constant temperature shifts in the gas hydrate phase boundary. This approach has two unknowns (thermal gradient and temperature shift of the phase boundary) and thus, by picking more than two depth levels of the BSR, is well constrained. In a trial-and-error approach, we found a good match for a thermal gradient of 0.027°C m^{-1}, a seafloor temperature of 0.0°C, and a BGHS pinchout at 605 m water depth (Figure 9). We estimated error margins based on trial-and-error models as ±0.002°C m^{-1} and ±20 m for thermal gradient and depth of the BGHS pinchout, respectively.

Average water temperatures are ~0.1°C lower in the Tuaheni area than on Rock Garden (and probably well within the error margin of observations), the equivalent of only ~4–5 m water depth at the predicted BGHS pinchout. Yet, BGHS pinchouts on Rock Garden were observed at a water depth of 630–645 m. A thermal

© 2014. American Geophysical Union. All Rights Reserved.

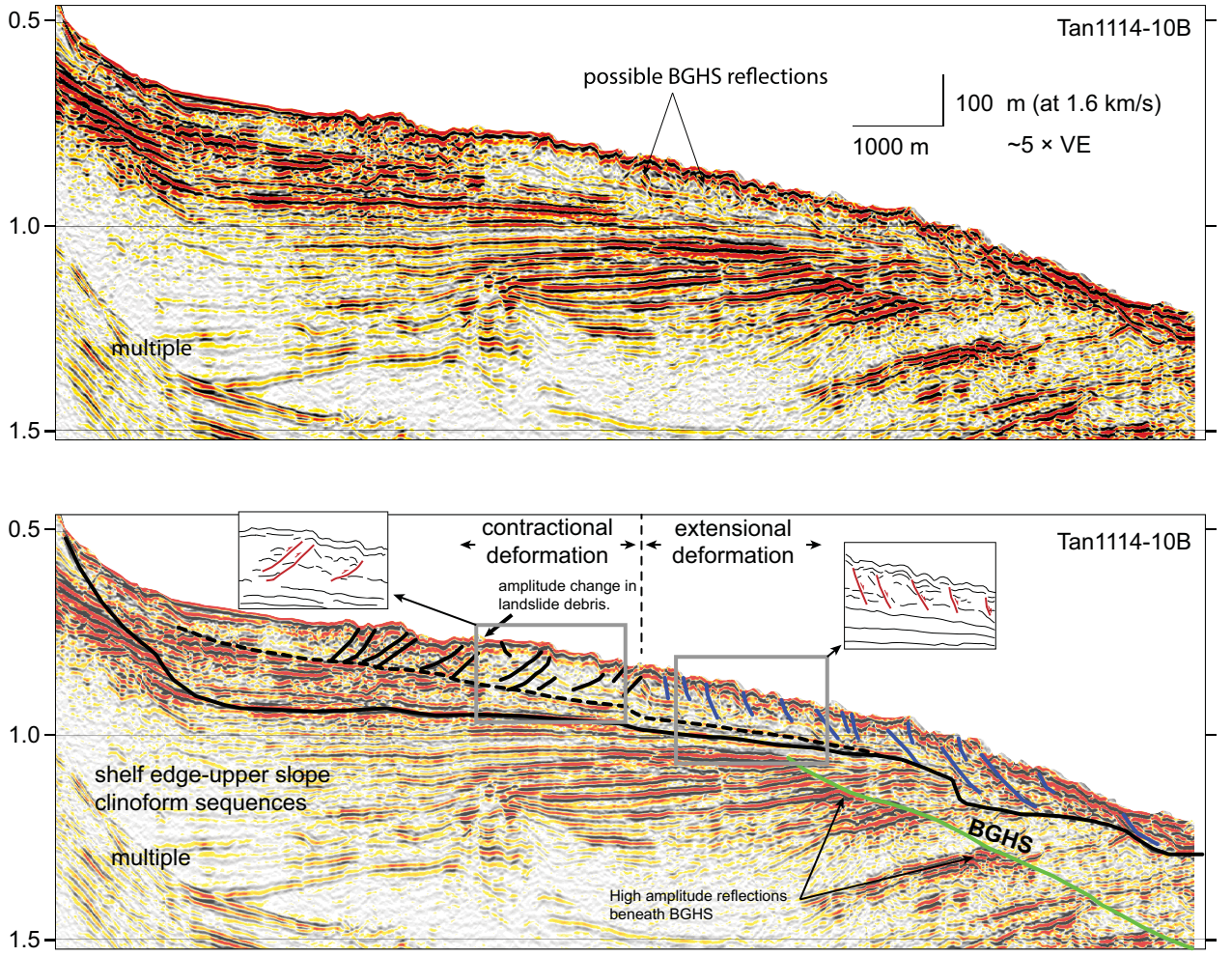

Figure 5. Uninterpreted and interpreted versions of true-amplitude multichannel seismic profile Tan1114-10B down the length of the Tuaheni landslide. Features mapped include the base of landslide debris (solid black line), the interpreted base of active deformation (dashed black line), and the base of gas hydrate stability (BSR, green), internal landslide deformation features (black). Linework interpretations show an internal reflectivity indicative of faulting style.

gradient of 0.020°C m^{-1} would be required for a BGHS pinchout at 630 m in order to match the predicted depth of the BGHS with the shallowest termination of a high-amplitude reflection (possible BGHS Figure 5). The predicted BGHS "dives" well below the observed termination of high-amplitude events at greater depths. *Pecher et al.* [2005] suggest that similar deviations between the predicted and observed curvature of the BGHS for given depths of BGHS pinchouts may be due to seismic resolution (the actual BGHS pinchout may be shallower but not resolved) or localized advective heatflow due to fluid expulsion at BGHS pinchouts leading to an increase of thermal gradient from $<$0.03°C m^{-1} on the flanks of Rock Garden to $>$0.05°C m^{-1} close to the BGHS pinchouts. Fluid expulsion is consistent with vigorous gas venting observed next to BGHS pinchouts on Rock Garden. In the absence of further data, we therefore estimate the BGHS pinchout for average water temperatures in the Tuaheni slide area to be present between 585 m (predicted minus estimated error margin) and 640 m (deepest BGHS pinchouts on Rock Garden adjusted for slightly lower temperatures in the Tuaheni area), with a maximum probability at 605 m. We note that the BGHS pinchout is predicted to fluctuate by almost $\pm$50 m as a function of bottom-water temperature variations probably on relatively short, mesoscale time scales.

Three observed depths of the BSR should thus be sufficient to allow prediction of the BGHS pinchout location. This approach has a number of additional unknowns, such as seismic velocity and thermal conductivity; however, we have demonstrated that even a change of predicted BGHS pinchout of 25 m (605–630 water depth) makes it difficult to match the observed depth profile of the BGHS. However, additional factors

© 2014. American Geophysical Union. All Rights Reserved.

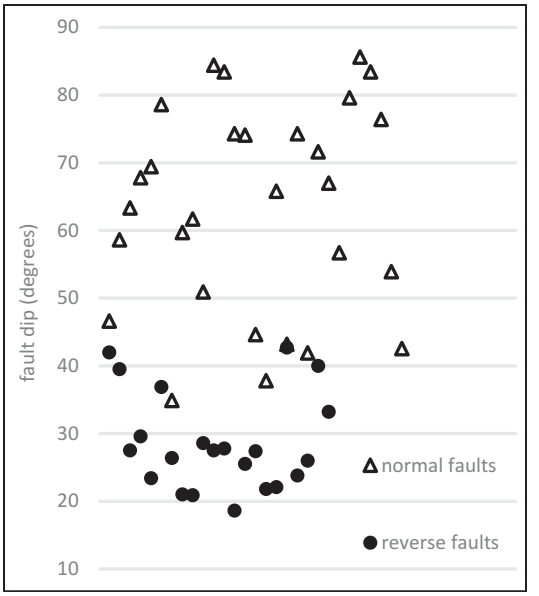

Figure 6. Plotted apparent dips of landslide debris faults interpreted in Figures 4 and 5. A distinction is made between contractional (reverse) and extensional (normal) faults. Back thrust (i.e., landward verging) contractional faults were not included in the analysis.

such as sedimentation rate and local advective-heatflow anomalies cannot be constrained, potentially leading to mismatches in the predicted depths of the BGHS and BSRs. We use the discrepancy between the predicted BGHS pinchout and observed BGHS pinchouts on Rock Garden based on BSRs (25–40 m) as a rough error measure for our predictions and hence conclude that the BGHS pinchout is in 605 $\pm$ 40 m water depth.

A constant shift of the phase boundary by -1°C at a gradient of 0.027°C m^{-1} would lead to a predicted BGHS roughly following the initial upper part of the observed shallower cross-cutting reflection (possible paleo BGHS in Figure 4). Further downslope, the predicted BGHS would reach a high-amplitude patch at the boundary between contractional and extensional deformation (Figure 5) that could be interpreted as gas at the BGHS. However, even further seaward, the predicted BGHS would be considerable deeper than the observed terminations of high-amplitude events that we interpret as marking the BGHS. If this reflection was a BSR, this mismatch between predicted and observed BGHS could best be explained by bottom-water cooling (or similarly, seafloor removal). In this case, the thermal field in the shallow subseafloor may already have readjusted to cooler conditions while the thermal pulse may not have reached deeper and thus, the depth of the BGHS may still be at its precooling level. Similarly, a deeper BGHS pinchout could be explained by a relatively recent increase of bottom-water temperatures by 1°C.

To obtain a rough estimate of the timescale of possible thermal disturbances (including sudden sediment deposition or removal), we modeled the penetration of a temperature step of $+1$°C into the seafloor. Significant temperature changes at 50 mbsf, roughly the depth that the shallower cross-cutting reflection are predicted to start between 20 and 100 years (Figure 10). At $\sim$115 mbsf, the shallowest depth of observed terminations of high-amplitude reflections interpreted as BSRs (top of green line Figures 4 and 5),

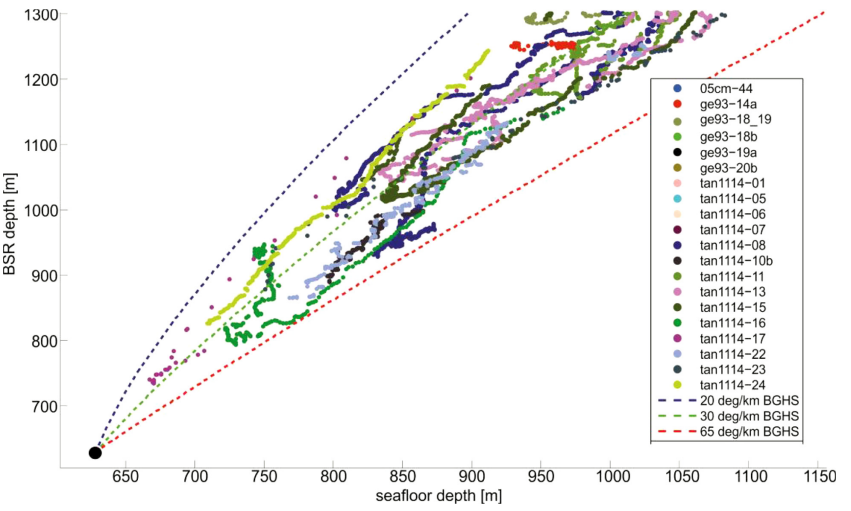

Figure 7. Base of gas hydrate stability indicators (BSR) mapped from seismic reflection profiles in the immediate region of the study area (i.e., white lines in Figure 1c indicate a location of seismic reflection profiles). Picks are plotted as seafloor depth against depth below seafloor. Modeled methane hydrate stability curves for three geothermal gradients are shown.

© 2014. American Geophysical Union. All Rights Reserved.

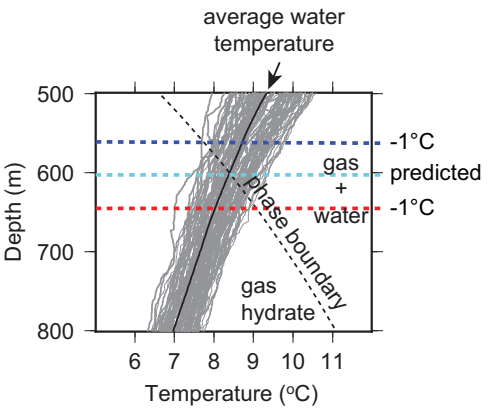

Figure 8. CTD measurements of water temperature plotted with the hydrate to gas and water phase boundary, and the BGHS pinchout for the present situation (light blue) and for a temperature fluctuation of plus and minus 1°C (red and dark blue lines, respectively). Colors of BGHS pinchout boundaries match those in Figure 9.

temperatures remain almost constant for about 200 years following the temperature step. Latent heat for gas hydrate dissociation and limited mobility of free gas would add to the time required for adjusting the position of the BSR after any temperature steps. Hence, if temperature steps caused a discrepancy between BGHS pinchout and the deeper BGHS, they would have occurred in the past several hundreds of years.

4. Discussion

Despite widespread inferences that gas hydrates have a significant role in seafloor instability, few hydrate-associated slope failure mechanisms have been proposed beyond the conventional model of gas hydrate dissociation at the BGHS destabilizing intact slopes. Given the complexity of hydrate and gas within GHSZ sediments [*Navalpakam et al*., 2012; *Suess et al*., 2001], the gas hydrate system is very likely to have numerous and varied influences on sediment stability and slope failure processes at a range of scales.

Our analyses indicate that the BGHS projects to the seafloor within an actively deforming submarine landslide. To facilitate "active" ongoing downslope deformation of landslide debris a dynamic and short-time scale trigger is required. Long-term average downslope deformation rates for terrestrial low-velocity active landslides show a remarkable consistency around 1 ± 0.5 m yr^{-1}. This is the case for precipitation forced movement in weak-rock earthflows [*Corsini et al*., 2005; *Mackey et al*., 2009], as well as for gravity forced movement in creeping flows composed of a sediment-ice mix [*Bodin et al*., 2008; *Haeberli et al*., 2006]. We infer that movement rates in the Tuaheni landslides should be in this range to maintain the geomorphic features that identify this as a low-velocity actively moving landslide. To quantify this movement rate in the future will require either a long-term program of very high resolution (e.g., Autonomous Underwater Vehicle or AUV) repeat bathymetric surveys, or the installation of a seafloor deformation monitoring network. Although seismic ground-shaking is likely to influence slope stability in this region, such a process does not provide stability perturbations on these shorter timescales considered a requirement to maintain an active low-velocity landslide complex (e.g., subdecadal). Our data and analysis lead us to the hypothesis that the shallow gas hydrate system provides the driving mechanism for this active landslide.

4.1. Development of the Tuaheni Landslide Complex

Many conceptual models exist for the emplacement of submarine landslide complexes. These include single event failures [*Lafuerza et al*., 2012], multiple events resulting in stacked debris sheets [*Greene et al*., 2006], small displacement sediment spreading [*Micallef et al*., 2007], and rapid runout mudflows [*Sawyer et al*., 2012]. Evidence for multiple catastrophic failures in the Tuaheni landslide complex includes the remnant lobe and lower debris unit interpreted as part of a parent failure (Figures 3–5), and the composite headscarp indicating multiple small scale failure (Figure 3). However, the conclusion of *Mountjoy et al*. [2009] that the internal structure and morphology of the present Tuaheni landslide complex does not show features consistent with multiple stacked events being solely responsible for constructing the landslide complex (e.g., coalescing lobes, debris units separated by coherent reflectivity in seismic

Table 1. Thermal Properties for Estimating the Propagation of a Temperature Step into the Seafloor[a]

	ρ (kg m^{-3})	k (W m^{-1} K^{-1})	Cp (J kg^{-1} s^{-1})
Pore water	1035	0.60	4187.00
Matrix	2650	2.80	750.00
Bulk	1647	1.08	2884.38

[a]Density (ρ), thermal conductivity (k), and specific heat (Cp) for sediment [*Fowler*, 1990]. Porosity estimated as 0.62 from a seismic velocity of 1600 m s^{-1} [*Hamilton*, 1978], k of the rock matrix is for a sandy shale [*Kappelmeyer and Haenel*, 1974]. Cp ranges between 500 and 1000 J kg^{-1} s^{-1} for marine sediments [*Schon*, 1996]—we therefore use 750 J kg^{-1} s^{-1} as average. These properties do not account for gas hydrates nor do the models incorporate latent heat needed for gas hydrate dissociation.

© 2014. American Geophysical Union. All Rights Reserved.

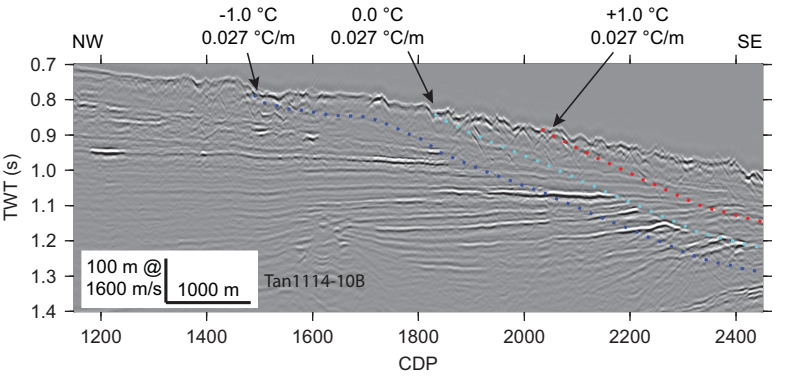

Figure 9. Location of the BGHS with respect to the seafloor for the current situation (0.0°C) and varying temperatures based on data from Figure 8. Curves are overlain on seismic reflection profile Tan1114-10B as per Figure 5.

reflection data) is supported by the new data presented in this study. This is true for the landslide deposits above the dashed line in Figures 4 and 5 (interpreted as the active portion of the failure complex), and we acknowledge that the unit below this line may contain multiple events.

Based on our data analysis, we propose three key steps in the evolution of an intact slope into the active landslide complex of the present day (Figure 11).

The Tuaheni landslide complex is proposed to have first occurred as a relatively large failure from the upper slope which ran out into the basin defined by Tuaheni Ridge, with the lower part coming to rest on gas hydrate-bearing sediments. This initial failure constitutes the first step in Figure 11a. The remnant toe of this frontally confined parent failure exhibits compressive structures (Figure 3) [*Mountjoy et al*., 2009] in accordance with widely accepted landslide emplacement models for both submarine and terrestrial landslide deposition, resulting in thinning and extensional deformation in the upper slide mass and contraction in the distal toe-area [*Bull et al*., 2009; *Prior et al*., 1984; *Turner and Schuster*, 1996]. Seismic reflection data reveal a lower, wedge-shaped unit underlying the main debris sheet that is interpreted as a remnant of this initial parent failure (Figures 4 and 5). This initial failure of the upper-slope clinoform sediments is most likely to have been earthquake triggered. The composite headscarp of the landslide complex indicates that it has formed by multiple failures and this likely reflects the ongoing development of the headscarp following the loss of lateral support after the initial failure.

Since landslide debris was deposited sufficiently far downslope to enter the field of gas hydrate stability (Figure 11a), the second key step (Figure 11b) involves the first interaction between the gas hydrate system and the failed material from the parent landslide. As a fluid flow system developed through the emplaced landslide debris, we expect gas hydrate to have formed within the pore spaces of the debris. Recent studies demonstrate the short time periods over which methane hydrates can colonize a sedimentary structure [*Berndt et al*., 2014]

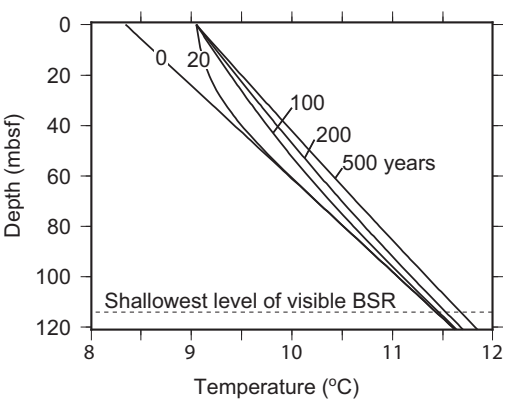

Figure 10. Modeled BGHS temporal response to changes in bottom-water temperatures. Plot illustrates how a dramatic seaward shift would occur at the shallowest BGHS in the early stages of bottom-water temperature warming, followed by more gradual change over time. The shallowest observed BSR in seismic reflection data is plotted.

Assuming that interstitial hydrate had formed within the landslide debris, it would potentially change the mechanical properties of the sediment in at least two ways. (1) Under rapid loading rates, the brittle strength of the sediment is likely to be increased [*Durham et al*., 2003]. This strength increase would limit the potential for further catastrophic failure of the landslide debris. In this case, it would provide something of a buttress to rapid static loading from material failing from the

© 2014. American Geophysical Union. All Rights Reserved.

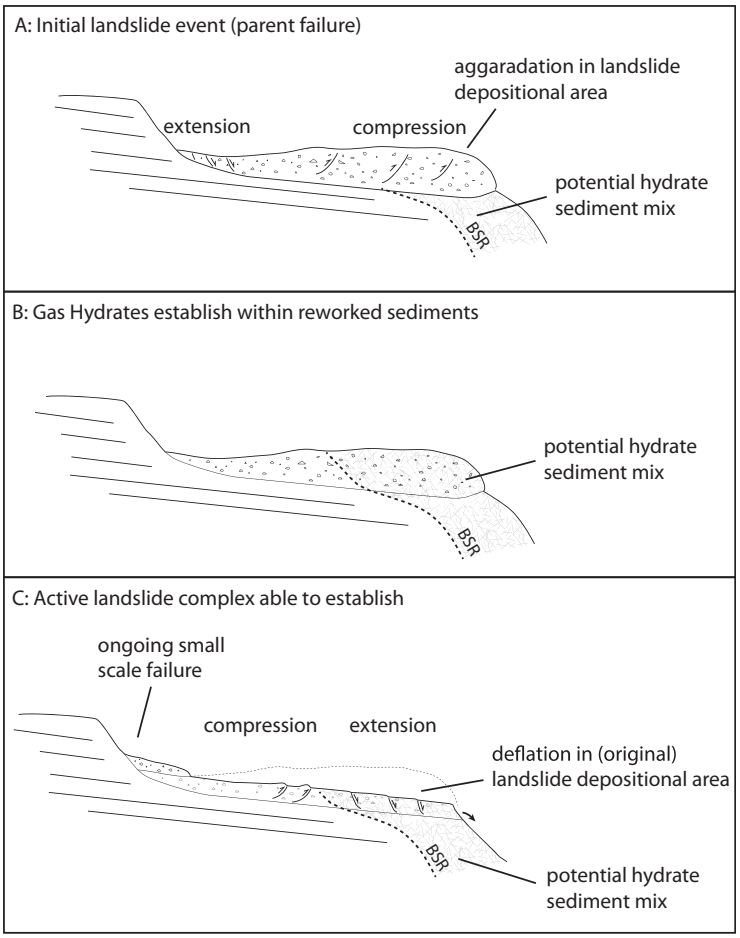

Figure 11. Cartoon illustrating the three key stages in the evolution from the intact Tuaheni slope to an active landslide complex. (a) The parent landslide occurs onto intact slope sediments. The post glacial gas hydrate system is established within the subseafloor and the TGHS would be at 600 m bsl. (b) Over time the gas hydrate system reestablishes to the new seafloor (the landslide surface) and interstitial hydrate may form within the landslide debris. (c) The slope evolves to the present-day situation with an active landslide complex. Note that from the initial failure, the distribution of extension versus contraction has switched so that extension now occurs in the downslope region of the failure.

headscarp upslope. (2) The sediment is likely to attain enhanced viscoplastic properties under low loading rates [*Miyazaki et al*., 2011]. This means the material may be susceptible to creep deformation. In addition, the development of interstitial hydrate is likely to alter the permeability characteristics of the sediment.

Our hypothesis is that once hydrate has formed within the landslide debris, the hydrate system provides a mechanism for active landsliding to occur (Figure 11c). The newly identified methane hydrate and underlying free gas system may provide a cyclic, short- time scale mechanism to perturb slope stability over prolonged time periods. The presence of this landslide type is believed to reflect a combination of preconditioning factors including sediment type and availability (stratified weak sediments) and slope geomorphology (gentle slope gradients, toe removal mechanisms). What is actually triggering and maintaining the proposed movement within the debris stream is the subject of this discussion in section 5.3, and we focus on formulating hypotheses for how the coincident gas and gas hydrate system might be facilitating active landslide movement.

4.2. Spatial Relationship Between Gas Hydrates and the Landslide Mass

Seismic reflection data and hydrate stability modeling indicate that the BGHS approaches the seafloor within the central zone of the Tuaheni landslides (Figures 7–9). While we cannot identify any unambiguous BGHS pinchouts, the modeled location of the BGHS occurs at between 585 and 640 m water depth (Figure 3). This modeled pinchout coincides with the transition between contraction and extension mapped in the

© 2014. American Geophysical Union. All Rights Reserved.

landslide complex and applies to the three components of the Tuaheni landslide complex. This indicates that interstitial hydrate could be incorporated into sediments in the extensional region of the landslides, within the underlying intact sequences and within the debris, and is very likely to occur in shallow sediments where the BGHS approaches the seafloor [e.g., *Tréhu et al*., 2004]. Below the BGHS, reservoirs of free gas and pressurized gas are known to occur [*Flemings et al*., 2003; *Hornbach et al*., 2004]. At Tuaheni, high-amplitude reflection packages that truncate against the BGHS indicate the presence of a free gas system.

The observation that hydrates are not involved with the upslope reaches of the slide departs from existing models of hydrates and slope failure [*Kvenvolden*, 1993; *Paull et al*., 1996]. As the initial landslides initiated well upslope of the gas hydrate zone, hydrate dissociation beneath the initial slide mass cannot be implicated as the trigger for the parent landslides. It is possible that hydrate dissociation-related failure initiated near the toe of the parent landslide and developed in a retrogressive fashion. However, it is more likely that the parent landslides occurred as a result of earthquake ground shaking, with other contributing factors such as sediment loading playing a role. The initial probably catastrophic failure is significantly different from the present situation, where the parent landslide has been remobilized as a creeping failure. We propose two models for the current slow deformation is either repeated remobilization or continual downslope creep of the emplaced debris. Explanation of this mobility requires either a constant driving force or a cyclic perturbation to reduce the static stability of the slope.

4.3. Influence of the Gas Hydrate System on Active Landsliding

The Tuaheni landslides demonstrate key attributes of relevance to the models we propose for hydrate-related instability. (1) The landslides are actively deforming [*Mountjoy et al*., 2009], either continuously or episodically in response to physical perturbations. (2) All lateral-shear-bounded "debris streams" within the failure complex have a free (unconfined) lower boundary where landslide debris can be removed. (3) The BSR is not coincident with the failure source area on the intact slope, but rather the BGHS is predicted to pinch out to the seafloor within the landslide debris. The coincidence of an active landslide complex and a gas hydrate system leads us to consider three mechanisms by which the gas hydrate system could control this little-known mode of submarine sediment instability. These three mechanisms are discussed in the following three subsections.

4.3.1. Gas Hydrate Dissociation

Dissociation of methane clathrate to methane gas and liquid water provides a mechanism for in-sediment pore pressure generation that has been widely considered in publications on the topic over the last 30+ years [*McIver*, 1982]. *Phrampus and Hornbach* [2012] have recently presented evidence indicating that bottom-water warming has resulted in a downward movement of the BGHS leading to gas hydrate dissociation, the generation of overpressured gas, and potentially to seafloor destabilization. For Tuaheni, the variation of the BGHS under different temperature regimes indicated that the location of the seafloor pinchout of the BGHS would be approximately 2 km upslope under a -1°C temperature change (Figure 9). This increased hydrate stability would yield a potential zone of excess pore pressure generation under parts of the slide debris further upslope (i.e., beneath the lower end of the contractional domain of the parent landslide) (Figure 12a). If this phase change occurred rapidly, it would certainly influence sediment stability. However, detracting from this mechanism is the timeframe over which such a process is likely to operate, in the absence of large seasonal ocean-temperature fluctuations, for example, as observed in arctic regions [*Berndt et al*., 2014]. Hydrate dissociation does not appear to provide a robust mechanism for triggering landslide movement, and is unlikely to provide ongoing perturbation to support such an actively deforming landslide complex. A water temperature decrease needed to match predicted BGHS and depth of the shallower cross-cutting reflection would lead to on-going gas hydrate formation, not dissociation, and thus would not be predicted to cause seafloor instability using this model.

4.3.2. The Hydrate Valve

The repeated formation and dissociation of gas hydrates following bottom-water-temperature fluctuations is proposed to cause seafloor weakening close to BGHS pinchouts [*Pecher et al*., 2005]. Modeling of this mechanism indicates that significant fluid overpressure can develop in the presence of fluid flow, assuming that gas hydrates in the pore spaces of sediments cause permeability reductions [*Crutchley et al*., 2010; *Ellis et al*., 2010]. Where the BGHS approaches the seafloor, pore pressure may reach lithostatic levels leading to hydrofracturing into the shallow gas hydrate zone [*Crutchley et al*., 2010]. As fractures develop, elevated

© 2014. American Geophysical Union. All Rights Reserved.

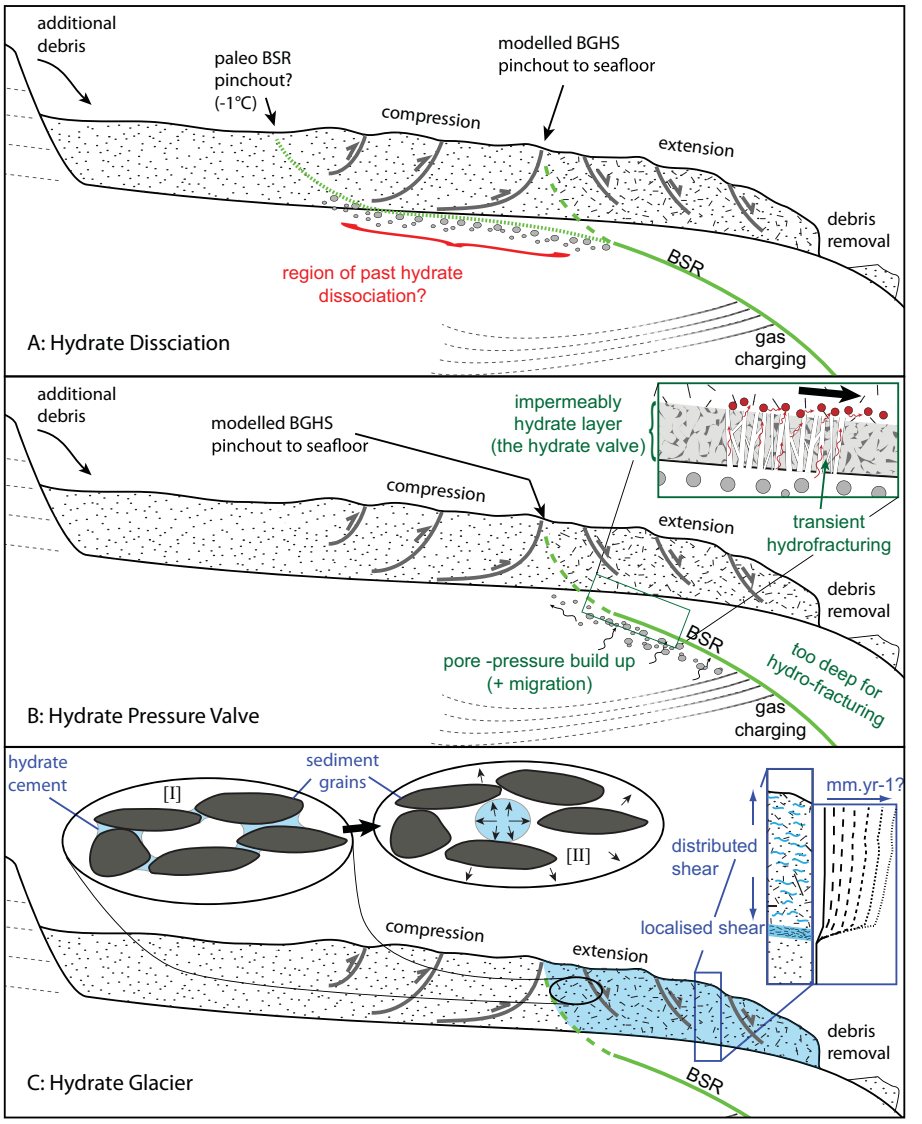

Figure 12. Schematic illustration of the three proposed models for hydrate-controlled active landsliding. (a) Hydrate dissociation due to changing bottom-water temperature. The schematic model illustrates a dissociation occurring in the region of the landslide upslope of the observed BGHS. This seaward move of the BSR of approximately 2 km requires a temperature increase in the order of 1°C (Figure 9). (b) Methane hydrates acting as a pressure valve. Pressure accumulation below the impermeable layer defined BGHS reaches lithostatic pressure and causes transient hydrofracturing (inset). At a certain point seaward, the thickness of overburden will become too great for pore pressure to be transmitted to the landslide base. (c) The hydrate glacier. Downslope of the BGHS pinchout conditional enable hydrate formation within the landslide body (Figure 11b). Grain cementation (inset I) strengthens sediment in the short term but under sustained load enables creep to occur. Interstitial hydrate also may force grains apart altering geotechnical and permeability properties of the sediment (inset II). Shear deformation within the landslide body may be localized along a basal decollement, or distributed within the slide mass, as illustrated in the velocity profile. The displacement profiles associated with this indicate rates of mm/yr as for rock glaciers and show a predominantly basal shear dominated situation with a minor component of distributed shear. Displacement velocity profile after *Arenson et al*. [2002].

pore pressure may also be transmitted into low permeability landslide debris and destabilize the landslide body, initiating movement [*Viesca and Rice*, 2012] (Figure 12b). As the BGHS dives rapidly below the seafloor, the region within which hydrofracturing can occur is limited by the ability of overpressure to fracture the hydrate seal and allow the vertical migration of pressurized fluids. That is, at greater subseafloor depths, the magnitude of excess fluid pressure required to approach lithostatic pressure increases.

In terrestrial earthflows, precipitation-induced pore pressure-increase triggers downslope displacement, which is arrested once sediment dilation occurs [*Iverson et al*., 2000; *Schulz et al*., 2009]. This pore pressure—dilatency feedback enables ephemeral but repeated downslope movement of the landslide debris,

© 2014. American Geophysical Union. All Rights Reserved.

and is the core of the hydrate valve hypothesis with respect to landslide mobility. As pore pressure increases at the base and within the landslide body, which rests very near to static equilibrium, displacement occurs. During displacement, fracturing and dilation occur and pore pressures dissipate. Once landslide motion ceases pore pressure must build up to lithostatic again before debris movement reoccurs. Cyclic pressure build up, rupture, and resealing enables repeated movement of the landslide debris.

Detracting from this model is the rapid thickening of overburden above the BSR as the BGHS dives into the sedimentary sequence beneath the basal surface of the landslide. Although we have not calculated the threshold overburden thickness for hydrofracturing at this location, for thickness greater than 100 m, hydrofracturing is unlikely [*Crutchley et al*., 2010]. For the relatively steeply dipping BSR observed beneath the Tuaheni slides, this depth limitation may reduce the likelihood that this mechanism is the dominant controlling factor in active landslide mobility. However, in the case, that there is a deeper preexisting fracture network subject to cyclic hydrofracturing this process may be viable to greater depths.

4.3.3. Rheology Controlled Hydrate-Sediment Glaciers

In a totally new model, we propose that the presence of gas hydrate within the landslide debris could be enabling low-velocity plastic deformation to occur, similar to that found in sediment and water-ice mix rock glaciers [*Arenson et al*., 2002]. The position of the BGHS immediately below the Tuaheni landslide indicates the presence of methane hydrates within the sediment matrix (Figure 12c). Rock glaciers similarly contain distributed water ice within sediment, the presence of which enables long-term plastic creep of the debris body downslope [*Ikeda and Matsuoka*, 2006], and the viscous behavior is due to the cumulative deformation of thermally controlled ice/rock mixtures [*Haeberli et al*., 2006]. The review of *Haeberli et al*. [2006] shows that the thickness of the active deformation layer in rock-glaciers varies between 0.5 and 3 m. Ice concentrations in active layers in rock glaciers are typically 40–70%; however, in finer grained materials creep deformation can be facilitated by very low concentrations of ice cementing sediment together [*Ikeda and Matsuoka*, 2006]. Morphologically, the presence of well-formed lateral shear zones, contractional and extensional zones and deflation of the central debris stream of the Tuaheni landslide complex is consistent with viscous glacier-like deformation (Figure 3).

Natural methane hydrate likely occurs within sediment as distributed lenses, veins and pockets [*Suess et al*., 2001], while laboratory experiments indicate that the mechanical properties of sediment-hydrate mixes are strongly controlled by hydrate formation mechanisms [*Priest et al*., 2009]. Hydrate cementation is likely to strongly affect physical properties even at low saturation, and here we suggest that hydrate cement may deform plastically leading to viscous deformation of bulk sediment while strengthening sediments during short-term deformation. We propose that the hydrate/sediment ratio in the Tuaheni landslides might enable material to deform as a brittle-plastic creeping mass, as opposed to coherent sediment accelerating downslope. Creep may be preferentially located in basal shear zones or distributed throughout the deforming landslide mass (Figure 12c). The conditions for hydrate-sediment-mix materials (i.e., downslope of the BGHS pinchout) coincides with the spatial distribution of extensional deformation within the landslide debris. Creep deformation is likely to be strongly dependent on the formation mechanisms and morphology of hydrate formed in fine grained materials.

Formation of gas hydrates in fine-grained sediments is poorly understood. Most studies of the effect of hydrate formation on sediment strength, both in the field and in the laboratory, have focused on coarser-grained sands as reservoir rocks. Seismic and geotechnical studies in the field and laboratory studies on natural samples appear to be converging to a model that gas hydrates form within the pore space without cementing grains [*Lee and Collett*, 2001; *Winters et al*., 2004; *Yun et al*., 2007]. Laboratory studies on sediments partly saturated with artificially formed hydrate on the other hand, often show the significant increase of elastic properties expected for grain-cementing gas hydrates. This apparent discrepancy has been attributed to the availability of water or gas for hydrate formation, laboratory studies of artificial hydrates formed in sands with constrained water supply appear to form grain cement, whereas constrained gas supply appears to have led to pore-filling hydrate [*Priest et al*., 2009].

Elsewhere on the Hikurangi Margin, slopes with similar sediment and slope-gradient ubiquitously do not have failed sediment retained within landslide scars. That is, if sediment fails, it catastrophically runs away downslope. If gas hydrates form as grain-contact cement rather than frame-supporting grains, even small percentages of gas hydrates are expected to lead to a significant increase in sediment strength for short-

© 2014. American Geophysical Union. All Rights Reserved.

term deformations (Figure 12c-I). This would stop catastrophic failure from occurring. We suggest that creeping could then be caused by the plastic behavior of gas hydrate cement under a sustained load.

Theoretical studies as well as field observations of veins, lenses, nodules, and other macroscopic gas hydrate occurrences indicate that gas hydrate in fine-grained sediments may displace grains (Figure 12c-II). Next to hydrophilic mineral surfaces, it may be energetically advantageous for hydrate to displace grains in order to increase accommodation space and minimize the surface area of the hydrate-water interface rather than overcome the capillary entry pressure for hydrate formation in small pore space [*Clennell et al*., 1999; *Henry et al*., 1999]. We here speculate that during this process of hydrate formation, grain displacement may cause weakening of cohesive bonds between grains in unconsolidated sediments and thus, weakening and potential failure of sediments. This process would be localized and ephemeral on larger time and spatial scales, this type of failure may then appear as creeping. We note that this process is complicated by the uncertainty of gas hydrate formation leading to a net-volume reduction or increase. A volume reduction is commonly assumed if gas hydrates form from water and free gas is supplied over longer distances—the incorporation of free gas with a much lower density than water into the hydrate structure is known to lead to significant volume reduction [*Sloan and Koh*, 2007]. A net-volume increase would facilitate this process: such an increase could be expected for hydrate formation from free gas that only locally comes out of solution. The net effect is then volume expansion during the phase transition from water to less dense hydrate, similar to ice. We speculate that a similar frost-heave-like process could be in place on Rock Garden [*Faure et al*., 2006], where gas hydrate growth in fractures close to the seafloor could lead to volume expansion in fractures although bubble streams from hydrocarbon seeps suggest excess free gas migrating through the seafloor with hydrate formation to lead to a net decrease of pore volume. Better understanding of the processes associated with gas hydrate formation in fine-grained, clay-bearing sediments is required for any firmer conclusions.

Based on our data, analysis and observations we support the rheological control of interstitial hydrate formation as controlling the active mobility of the Tuaheni landslide complex. Active seafloor glacial processes controlled by interstitial hydrate could conceivably occur anywhere that hydrates are present at shallow depths in the sediment column. While more work is required to evaluate these hypotheses, through our existing data analysis we propose that hydrate-sediment glaciers may be a fundamental dynamic element of the marine cryosphere, and play a globally important role in continental margin stability with significant implications for resource exploitation, engineering infrastructure, and natural hazard assessments.

5. Conclusions

Traditional models of seafloor mass failure involve rapid mobility of sediment downslope in individual events. On land, and inferred on other planets, many processes involve the slow downslope creep of sediment-ice mixtures. We now see evidence that this type of process is occurring on the seafloor facilitated by gas hydrates. This constitutes a reversal in the perception of the role of gas in sediment strength in that gas hydrates may lead to creep rather than stabilization of the seafloor. This process has major implications for our understanding of sediment transport, landform development, hazards, and the role of gas hydrates in the seafloor environment.

Seismic reflection and bathymetry data show extension and deformation in the reverse locations to single event emplaced landslides. Normal faulting indicates that extensional deformation is occurring through the distal region of the landslide and this is coincident with the area where interstitial hydrate can form within the shallow sedimentary sequence. Hydrate indicators are observed throughout the area and both geometrical projection and modeling indicate that the base of gas hydrate stability (BGHS) would intersect the seafloor at 600 $\pm$ 50 m water depth. This is coincident with the downslope transition from contraction to extension within debris across the landslide complex. Multichannel seismic data indicate gas build up beneath the BGHS and features that may represent previous locations of the BGHS.

We propose three mechanisms by which the shallow gas hydrate system could be controlling this unique active landslide complex where extensional creep occurs in the distal extent of the debris field: (1) the widely cited model of gas hydrate dissociation, (2) hydrofracturing of hydrate-bearing sediments releasing excess pore pressure into the landslide mass, and (3) a new hypothesis that hydrates are facilitating viscoplastic glacial deformation.

© 2014. American Geophysical Union. All Rights Reserved.

While the "seafloor glacier" hypothesis remains unproven, the model best fits our observations and modeling, and we believe that this is a very exciting and potentially very important concept in seafloor process research. We propose that the poorly understood rheological properties of gas hydrate-sediment mixes are enabling this landslide to evolve into an active sedimentary transport system that is progressively or episodically moving material through the landslide zone in the manner of a terrestrial rock glacier.

Given the sensitivity of marine gas hydrate systems to temperature and pressure changes, future ocean temperature variations as well as sea-level changes could significantly affect the behavior of the hydrate-bearing marine slopes. This model for slope failure represents a paradigm shift for submarine landslide processes, and the influence of gas hydrates on slope stability. It is possible that this type of failure occurs widely where the marine gas hydrate system approaches the seafloor on continental margins, and acceptance of hydrate controlled active landslides would require a global reevaluation of seafloor instability processes within the hydrate pinchout zone.

Acknowledgments

This study has been supported by the New Zealand Ministry of Business Innovation and Employment (MBIE) Crown Research Institute Core funding to NIWA and GNS Science and LINZ Oceans 2020 ship time. We are grateful to the Officers and Crew of RV Tangaroa for their excellent work during voyage Tan1114. We thank Steve Chiswell at NIWA for providing CTD data and Jim McKean at the USFS for insightful discussions on the topic. The contributions of two anonymous reviewers made significant improvements to this paper.

References

Alexander, C. R., J. P. Walsh, and A. R. Orpin (2010), Modern sediment dispersal and accumulation on the outer Poverty continental margin, *Mar. Geol.*, *270*, 213–226.

Arenson, L., M. Hoelzle, and S. Springman (2002), Borehole deformation measurements and internal structure of some rock glaciers in Switzerland, *Permafrost Periglac. Processes*, *13*, 117–135, doi:10.1002/ppp.414.

Barnes, P. M., K. Ching Cheung, A. P. Smits, G. Almagor, S. A. L. Read, P. R. Barker, and P. C. Froggatt (1991), Geotechnical analysis of the Kidnappers Slide, upper continental slope, New Zealand, *Mar. Geotechnol.*, *10*, 159–188.

Barnes, P. M., A. Nicol, and T. Harrison (2002), Late Cenozoic evolution and earthquake potential of an active listric thrust complex above the Hikurangi subduction zone, New Zealand, *Geol. Soc. Am. Bull.*, *114*(11), 1379–1405.

Barnes, P. M., G. Lamarche, J. Bialas, S. Henrys, I. A. Pecher, G. L. Netzeband, J. Greinert, J. J. Mountjoy, K. Pedley, and G. Crutchley (2010), Tectonic and geological framework for gas hydrates and cold seeps on the Hikurangi Subduction Margin, New Zealand, *Mar. Geol.*, *272*(1–4), 26–48.

Barnes, P. M., et al. (2011), National Institute of Water and Atmospheric Research (NIWA) Voyage Report, Ocean 2020 Northern Hikurangi Margin Geohazards, *RV Tangaroa Rep. Tan1114*, NIWA, Wellington, New Zealand.

Baum, R., W. Savage, and J. Wasowski (2003), Mechanics of earthflows, paper presented at International Conference Flows, IC-FSM2003, Sorrento, Italy.

Beavan, J., P. Tregoning, M. Bevis, T. Kato, and C. Meertens (2002), Motion and rigidity of the Pacific Plate and implications for plate boundary deformation, *J. Geophys. Res.*, *107*(B10), 2261, doi:10.1029/2001JB000282.

Berndt, C., S. Bünz, T. Clayton, J. Mienert, and M. Saunders (2004), Seismic character of bottom simulating reflectors: Examples from the mid-Norwegian margin, *Mar. Pet. Geol.*, *21*(6), 723–733.

Berndt, C., T. Feseker, T. Treude, S. Krastel, V. Liebetrau, H. Niemann, V. J. Bertics, I. Dumke, K. Dünnbier, and B. Ferré (2014), Temporal constraints on hydrate-controlled methane seepage off Svalbard, *Science*, *343*(6168), 284–287.

Bodin, X., P. Schoeneich, S. Jaillet, J. Delannoy, E. Ployon, B. Sadier, P. Deline, M. Arattano, M. Chiarle, and E. Cremonese (2008), *High-Resolution DEM Extraction from Terrestrial LIDAR Topometry and Surface Kinematics of the Creeping Alpine Permafrost: The Laurichard Rock Glacier Case Study (Southern French Alps)*, vol. 1, pp. 137–142, in Permafrost: Proceedings of the 9th international conference on permafrost, Inst. of Northern Eng., Univ. of Fairbanks, Alaska.

Bull, S., J. Cartwright, and M. Huuse (2009), A review of kinematic indicators from mass-transport complexes using 3D seismic data, *Mar. Pet. Geol.*, *26*(7), 1132–1151.

Chiswell, S. M. (2005), Mean and variability in the wairarapa and Hikurangi Eddies, *New. Zeal. J. Mar. Fresh.*, *39*(1), 121–134, New Zealand.

Clennell, M. B., M. Hovland, J. S. Booth, P. Henry, and W. J. Winters (1999), Formation of natural gas hydrates in marine sediments: 1. Conceptual model of gas hydrate growth conditioned by host sediment properties, *J. Geophys. Res.*, *104*(B10), 22,985–23,003.

Collett, T. S. (2002), Energy resource potential of natural gas hydrates, *AAPG Bull.*, *86*(11), 1971–1992.

Collot, J.-Y., et al. (1996), From oblique subduction to intra-continental transpression; structures of the southern Kermadec-Hikurangi margin from multibeam bathymetry, side-scan sonar and seismic reflection, *Mar. Geophys. Res.*, *18*(2–4), 357–381.

Collot, J.-Y., K. B. Lewis, G. Lamarche, and S. E. Lallemand (2001), The giant Ruatoria debris avalanche on the northern Hikurangi Margin, New Zealand: Result of oblique seamount subduction, *J. Geophys. Res.*, *106*(B9), 19,271–219,297.

Corsini, A., A. Pasuto, M. Soldati, and A. Zannoni (2005), Field monitoring of the Corvara landslide (Dolomites, Italy) and its relevance for hazard assessment, *Geomorphology*, *66*(1–4), 149–165.

Crutchley, G. J., S. Geiger, I. A. Pecher, A. R. Gorman, H. Zhu, and S. A. Henrys (2010), The potential influence of shallow gas and gas hydrates on sea floor erosion of Rock Garden, an uplifted ridge offshore of New Zealand, *Geo Mar. Lett.*, *30*(3–4), 283–303.

Davy, B., I. Pecher, R. Wood, L. Carter, and K. Gohl (2010), Gas escape features off New Zealand: Evidence of massive release of methane from hydrates, *Geophys. Res. Lett.*, *37*, L21309, doi:10.1029/2010GL045184.

de Vera, J., P. Granado, and K. McClay (2010), Structural evolution of the Orange Basin gravity-driven system, offshore Namibia, *Mar. Pet. Geol.*, *27*(1), 223–237.

Durham, W. B., S. H. Kirby, L. A. Stern, and W. Zhang (2003), The strength and rheology of methane clathrate hydrate, *J. Geophys. Res.*, *108*(B4), 2182, doi:10.1029/2002JB001872.

Ellis, S., I. Pecher, N. Kukowski, W. Xu, S. Henrys, and J. Greinert (2010), Testing proposed mechanisms for seafloor weakening at the top of gas hydrate stability on an uplifted submarine ridge (Rock Garden), New Zealand, *Mar. Geol.*, *272*(1–4), 127–140.

Faure, K., J. Greinert, I. A. Pecher, I. J. Graham, G. J. Massoth, C. E. J. De Ronde, I. C. Wright, E. T. Baker, and E. J. Olson (2006), Methane seepage and its relation to slumping and gas hydrate at the Hikurangi margin, New Zealand, *N. Z. J. Geol. Geophys.*, *49*(4), 503–516.

Field, B. D., et al. (1997), Cretaceous-Cenozoic geology and petroleum systems of the East Coast region, Monograph 19, 301 p., Inst. of Geol. and Nuclear Sci., New Zealand.

Flemings, P. B., X. L. Liu, and W. J. Winters (2003), Critical pressure and multiphase flow in Blake Ridge gas hydrates, *Geology*, *31*(12), 1057–1060.

© 2014. American Geophysical Union. All Rights Reserved.

Fowler, C. M. R. (1990), *The Solid Earth: An Introduction to Global Geophysics*, Cambridge Univ. Press, Cambridge, U. K.
Garfunkel, Z., A. Arad, and G. Almagor (1979), The Palmachim disturbance and its region setting, *Geol. Surv. Isr. Bull., 72*, 1–56, Jerusalem.
Glastonbury, J., and R. Fell (2008), Geotechnical characteristics of large slow, very slow, and extremely slow landslides, *Can. Geotech. J.*, *45*(7), 984–1005.
Greene, H. G., L. Y. Murai, P. Watts, N. A. Maher, M. A. Fisher, C. E. Paull, and P. Eichhubl (2006), Submarine landslides in the Santa Barbara Channel as potential tsunami sources, *Nat. Hazards Earth Syst. Sci.*, *6*(1), 63–88.
Haeberli, W., et al. (2006), Permafrost creep and rock glacier dynamics, *Permafrost Periglacial Processes*, *17*, 189–214, doi:10.1002/ppp.561.
Hamilton, E. L. (1978), Sound velocity-density relations in sea-floor sediments and rocks, *J. Acoust. Soc. Am.*, *63*, 366.
Henry, P., M. Thomas, and M. B. Clennell (1999), Formation of natural gas hydrates in marine sediments: 2. Thermodynamic calculations of stability conditions in porous sediments, *J. Geophys. Res.*, *104*(B10), 23,005–23,022.
Hornbach, M. J., D. M. Saffer, and W. S. Holbrook (2004), Critically pressured free-gas reservoirs below gas-hydrate provinces, *Nature*, *427*(6970), 142–144.
Hungr, O., S. Evans, M. Bovis, and J. Hutchinson (2001), A review of the classification of landslides of the flow type, *Environ. Eng. Geosci.*, *7*(3), 221–238.
Ikeda, A., and N. Matsuoka (2006), Pebbly versus bouldery rock glaciers: Morphology, structure and processes, *Geomorphology*, *73*(3–4), 279–296.
Iverson, R. M., M. E. Reid, N. R. Iverson, R. G. LaHusen, M. Logan, J. E. Mann, and D. L. Brien (2000), Acute sensitivity of landslide rates to initial soil porosity, *Science*, *290*(5491), 513–516.
Kappelmeyer, O., and R. Haenel (1974), Geothermics with special reference to application, *Berlin Gebrueder Borntraeger Geoexploration Monogr. Ser. 4*, 31 pp., Gebrueder Borntraeger, Berlin.
Kennett, J. P., K. G. Cannariato, I. L. Hendy, and R. J. Behl (2000), Carbon isotopic evidence for methane hydrate instability during quaternary interstadials, *Science*, *288*(5463), 128–133.
Kennett, J., K. G. Cannariato, I. L. Hendy, and R. J. Behl (2003), *Methane Hydrates in Quaternary Climate Change: The Clathrate Gun Hypothesis*, AGU, Washington, D. C.
Kukowski, N., J. Greinert, and S. Henrys (2010), Morphometric and critical taper analysis of the Rock Garden region, Hikurangi Margin, New Zealand: Implications for slope stability and potential tsunami generation, *Mar. Geol.*, *272*, 141–153.
Kvenvolden, K. A. (1993), Gas hydrates-geological perspective and global change, *Rev. Geophys.*, *31*(2), 173–187.
Lafuerza, S., N. Sultan, M. Canals, G. Lastras, A. Cattaneo, J. Frigola, S. Costa and C. Berndt (2012), Failure mechanisms of Ana Slide from geotechnical evidence, Eivissa Channel, Western Mediterranean Sea, *Mar. Geol.*, *307*, 1–21.
Lee, M. W., and T. S. Collett (2001), Elastic properties of gas hydrate-bearing sediments, *Geophysics*, *66*(3), 763–771.
Lopez, C., G. Spence, R. Hyndman, and D. Kelley (2010), Frontal ridge slope failure at the northern Cascadia margin: Margin-normal fault and gas hydrate control, *Geology*, *38*(11), 967–970.
Mackey, B. H., J. J. Roering, and J. A. McKean (2009), Long-term kinematics and sediment flux of an active earthflow, Eel River, California, *Geology*, *37*(9), 803–806.
Maloney, D., R. Davies, J. Imber, and S. King (2012), Structure of the footwall of a listric fault system revealed by 3D seismic data from the Niger Delta, *Basin Res.*, *24*(1), 107–123.
McIver, R. D. (1982), Role of naturally occurring gas hydrates in sediment transport, *AAPG Bull.*, *66*(6), 789–792.
Micallef, A., D. G. Masson, C. Berndt, and D. A. V. Stow (2007), Morphology and mechanics of submarine spreading: A case study from the Storegga Slide, *J. Geophys. Res.*, *112*, F03023, doi:10.1029/2006JF000739.
Micallef, A., J. J. Mountjoy, M. Canals, and G. Lastras (2012), Deep-seated bedrock landslides and submarine canyon evolution in an active tectonic margin: Cook Strait, New Zealand, in *Submarine Mass Movements and Their Consequences*, vol. 31, edited by Y. Yamada et al., pp. 201–212, Springer, Netherlands.
Mitchell, N. C., M. Ligi, V. Ferrante, E. Bonatti, and E. Rutter (2010), Submarine salt flows in the central Red Sea, *Geol. Soc. Am. Bull.*, *122*(5–6), 701–713.
Miyazaki, K., T. Yamaguchi, Y. Sakamoto, and K. Aoki (2011), Time-dependent behaviors of methane-hydrate bearing sediments in triaxial compression test, *Int. J. JCRM*, *7*(1), 43–48.
Mountjoy, J. J., and P. M. Barnes (2011), Active upper-plate thrust faulting in regions of low plate-interface coupling, repeated slow slip events, and coastal uplift: Example from the Hikurangi Margin, New Zealand, *Geochem. Geophys. Geosyst.*, *12*, Q01005, doi:10.1029/2010GC003326.
Mountjoy, J. J., and A. Micallef (2012), Polyphase emplacement of a 30 km^3 blocky debris avalanche and its role in slope-gully development, in *Submarine Mass Movements and Their Consequences*, vol. 31, edited by Y. Yamada et al., pp. 213–222, Springer, Netherlands.
Mountjoy, J. J., J. McKean, P. M. Barnes, and J. R. Pettinga (2009), Terrestrial-style slow-moving earthflow kinematics in a submarine landslide complex, *Mar. Geol.*, *267*(3–4), 114–127.
Multiwave (2005), 05CM 2D seismic survey, offshore East Coast-North Island, N. Z. *Openfile Pet. Rep. 3136*, Ministry Econ. Dev., Wellington, New Zealand.
Navalpakam, R. S., I. A. Pecher, and T. Stern (2012), Weak and segmented bottom simulating reflections on the Hikurangi Margin, New Zealand—Implications for gas hydrate reservoir rocks, *J. Pet. Sci. Eng.*, *88–89*, 29–40.
Paull, C. K., W. Ussler, and W. P. Dillon (1991), Is the extent of glaciation limited by marine gas-hydrates?, *Geophys. Res. Lett.*, *18*(3), 432–434.
Paull, C. K., W. J. Buelow, W. Ussler Iii, and W. S. Borowski (1996), Increased continental-margin slumping frequency during sea-level lowstands above gas hydrate-bearing sediments, *Geology*, *24*(2), 143–146.
Pecher, I., and S. Henrys (2003), *Potential Gas Reserves in Gas Hydrate Sweet Spots on the Hikurangi Margin*, Inst. of Geol. and Nuclear Sci., New Zealand.
Pecher I. A., S. A. Henrys, S. Ellis, G. Crutchley, M. Fohrmann, A. R. Gorman, J. Greinert, S. M. Chiswell (2005), TAN0607 Scientific Party, SO191 Scientific Party 2008. Erosion of seafloor ridges at the top of the gas hydrate stability zone, Hikurangi margin, New Zealand–New insights from research cruises between 2005 and 2007. Proc. 6th International Conference on Gas Hydrates, 10 pp., Vancouver.
Pecher, I. A., et al. (2010), Focussed fluid flow on the Hikurangi Margin, New Zealand—Evidence from possible local upwarping of the base of gas hydrate stability, *Mar. Geol.*, *272*(1–4), 99–113.
Pedley, K. L., P. M. Barnes, J. R. Pettinga, and K. B. Lewis (2010), Seafloor structural geomorphic evolution of the accretionary frontal wedge in response to seamount subduction, Poverty Indentation, New Zealand, *Mar. Geol.*, *270*(1–4), 119–138.
Phrampus, B. J., and M. J. Hornbach (2012), Recent changes to the Gulf Stream causing widespread gas hydrate destabilization, *Nature*, *490*(7421), 527–530.

© 2014. American Geophysical Union. All Rights Reserved.

Posamentier, H. W., and P. R. Vail (1988), Eustatic controls on clastic deposition II—Sequence and systems tract models, in *Sea-Level Changes: An Integrated Approach*, vol. 42, edited by C. K. Wilgus et al., pp. 125–154, Soc. of Econ. Paleontol. and Miner. Spec. Publ.
Priest, J. A., E. V. Rees, and C. R. Clayton (2009), Influence of gas hydrate morphology on the seismic velocities of sands, *J. Geophys. Res.*, *114*, B11205, doi:10.1029/2009JB006284.
Prior, D. B., B. D. Bornhold, and M. W. Johns (1984), Depositional characteristics of submarine debris flow, *J. Geol.*, *92*, 707–727.
Sawyer, D. E., P. B. Flemings, J. Buttles, and D. Mohrig (2012), Mudflow transport behavior and deposit morphology: Role of shear stress to yield strength ratio in subaqueous experiments, *Mar. Geol.*, *307–310*, 28–39.
Scholz, C. H. (2002), *The Mechanics of Earthquakes and Faulting*, Cambridge Univ. Press, Cambridge, U. K.
Schon, J. H. (1996), *Physical Properties of Rocks: Fundamentals and Principles of Petrophysics*, Pergamon, Oxford, U. K.
Schulz, W., J. McKenna, J. Kibler, and G. Biavati (2009), Relations between hydrology and velocity of a continuously moving landslide—Evidence of pore-pressure feedback regulating landslide motion?, *Landslides*, *6*(3), 181–190.
Sloan, E. D., and C. A. Koh (2007), *Clathrate Hydrates of Natural Gases*, 721 p., Marcel Bekker, N. Y.
Stirling, M., et al. (2012), National seismic hazard model for New Zealand: 2010 update, *Bull. Seismol. Soc. Am.*, *102*(4), 1514–1542.
Suess, E., et al. (2001), *Sea Floor Methane Hydrates at Hydrate Ridge, Cascadia Margin, Natural Gas Hydrates: Occurrence, Distribution, and Detection*, vol. 124, pp. 87–98, AGU, Washington, D. C.
Sultan, N. (2007), Comment on "Excess pore pressure resulting from methane hydrate dissociation in marine sediments: A theoretical approach" by Wenyue Xu and Leonid N. Germanovich, *J. Geophys. Res.*, *112*, B02103, doi:10.1029/2006JB004527.
Sultan, N., and S. Garziglia (2011), Geomechanical constitutive modelling of gas-hydrate-bearing sediments, paper presented at 7th International Conference on Gas Hydrates, ICGH 2011, Edinburgh, U. K.
Sultan, N., P. Cochonat, J. P. Foucher, and J. Mienert (2004), Effect of gas hydrates melting on seafloor slope instability, *Mar. Geol.*, *213*(1–4), 379–401.
Tréhu, A. M., et al. (2004), Three-dimensional distribution of gas hydrate beneath southern Hydrate Ridge: Constraints from ODP Leg 204, *Earth Planet. Sci. Lett.*, *222*(3–4), 845–862.
Turner, A. K., and R. L. Schuster (1996), *Landslides: Investigation and Mitigation*, 673 pp., Natl. Acad. Press, Washington, D. C.
Van Wagoner, J. C., H. W. Posamentier, R. M. Mitchum, P. R. Vail, J. F. Sarg, T. S. Loutit, and J. Hardenbol (1988), An overview of the fundamentals of sequence stratigraphy and key definitions, in *Sea-Level Changes: An Integrated Approach*, vol. 42, edited by C. K. Wilgus, pp. 39–44, Soc. of Econ. Paleontol. and Miner. Spec. Publ.
Viesca, R. C., and J. R. Rice (2012), Nucleation of slip-weakening rupture instability in landslides by localized increase of pore pressure, *J. Geophys. Res.*, *117*, B03104, doi:10.1029/2011JB008866.
Vogt, P. R., and W. Y. Jung (2002), Holocene mass wasting on upper non-Polar continental slopes—Due to post-Glacial ocean warming and hydrate dissociation?, *Geophys. Res. Lett.*, *29*(9), 1341, doi:10.1029/2001GL013488.
Wallace, L. M., J. Beavan, R. McCaffrey, and D. Darby (2004), Subduction zone coupling and tectonic block rotations in the North Island, New Zealand, *J. Geophys. Res.*, *109*, B12406, doi:10.1029/2004JB003241.
Westbrook, G. K., K. E. Thatcher, E. J. Rohling, A. M. Piotrowski, H. Pälike, A. H. Osborne, E. G. Nisbet, T. A. Minshull, M. Lanoisellé, and R. H. James (2009), Escape of methane gas from the seabed along the West Spitsbergen continental margin, *Geophys. Res. Lett.*, *36*, L15608, doi:10.1029/2009GL039191.
Winters, W. J., I. A. Pecher, W. F. Waite, and D. H. Mason (2004), Physical properties and rock physics models of sediment containing natural and laboratory-formed methane gas hydrate, *Am. Mineral.*, *89*(8–9), 1221–1227.
Winters, W. J., W. F. Waite, D. H. Mason, L. Y. Gilbert, and I. A. Pecher (2007), Methane gas hydrate effect on sediment acoustic and strength properties, *J. Pet. Sci. Eng.*, *56*(1–3), 127–135.
Wysoczanski, R., et al. (2012), R.V. Tangaroa Research Voyage Report, *NIRVANA Rep. TAN1213*, National Institute of Water and Atmospheric Research (NIWA), Wellington, New Zealand.
Xu, W. Y., and L. N. Germanovich (2006), Excess pore pressure resulting from methane hydrate dissociation in marine sediments: A theoretical approach, *J. Geophys. Res.*, *111*, B01104, doi:10.1029/2004JB003600.
Yun, T. S., J. C. Santamarina, and C. Ruppel (2007), Mechanical properties of sand, silt, and clay containing tetrahydrofuran hydrate, *J. Geophys. Res.*, *112*, B04106, doi:10.1029/2006JB004484.

© 2014. American Geophysical Union. All Rights Reserved.